JET–P(99)45

L C Ingesson et al

Characterization of Geometrical Detection-system Properties for Two-dimensional Tomography

JET–P(99)45

Characterization of Geometrical Detection-system Properties for Two-dimensional Tomography

L C Ingesson, C F Maggi, R Reichle[1].

JET Joint Undertaking, Abingdon, Oxfordshire, OX14 3EA,
[1]Present address: CEA Cadarache, 13108 Saint-Paul-lez-Durance, France.

Preprint of a Paper published in
Review of Scientific Instruments **71**, 1370-1378 (2000)

December 1999

ABSTRACT

Quantities that characterize the three-dimensional geometrical properties of detection systems for two-dimensional tomography are reviewed and compared. It is discussed how the quantities can be calculated and how they can be measured, including a measuring technique that uses a parallel laser beam. In many detection systems the finite detector size and the finite sizes of bounding apertures are not negligible, and these result in instrument functions with finite widths. Line-integral measurements are referred to as ideal measurements, whereas measurements by systems with instrument functions with finite width are non-ideal. The quantities discussed make it possible to take into account these finite sizes in several tomography algorithms. If the spacing between adjacent lines of sight is much smaller than the widths of the instrument functions, the ideal measurements can be approximately reconstructed from the non-ideal measurements. Such a reconstruction has been applied to bolometer measurements in a high plasma-density discharge in the JET (Joint European Torus) tokamak by sweeping the plasma in front of the bolometer detectors. The sweeping creates many extra virtual lines of sight and thus increases the resolution of the measurements close to the X point, where in high-density plasmas a peak in the radiation is found.

PACS numbers: 42.30.Wb, 42.79.Ag, 52.70.Kz, 52.25.Qt

1. INTRODUCTION

The measurements by detection systems used for emission computerized tomography are often assumed to be along infinitely thin straight lines (straight lines if refraction is negligible). This approximation with straight lines can be satisfactory if the sizes of detectors and apertures are negligible. We will refer to such line-integral measurements as ideal. Experimentally, to achieve a good signal to noise ratio and coverage without gaps, however, it is often necessary to use detectors and apertures with sizes that are not negligible, which leads to non-ideal measurements along beams with finite widths. Note that non-ideal does not mean undesirable, since, apart from improving the signal-to-noise ratio, the finite widths also reduce aliasing of high-frequency spatial components.[1–3] Several methods exist to characterize the detection system with such finite sizes, so that the full three-dimensional detection-system properties can be taken into account in algorithms for two-dimensional tomography. These methods are briefly reviewed and efficient methods to calculate and measure the appropriate detection-system properties are presented (Sec. 3). Examples of these methods are given for the pinhole and collimator detectors of the bolometer-tomography system (described in Sec. 2) on the JET (Joint European Torus) tokamak, a device for nuclear fusion research.

A convenient way to describe the geometrical properties of the detection system is with the geometric function. The geometric function describes the solid angle spanned by the entrance pupil of the detection system for each position in the reconstruction region (i.e. the region in which we wish to reconstruct the local emissivity); to make the distinction between this function

and another geometric function discussed later, this function will be referred to as the geometric function in reconstruction space. If the viewing geometry, i.e. the positions and sizes of the detectors and apertures (and lenses if applicable), is known accurately, the geometric function in reconstruction space can be calculated. An efficient method to calculate the geometric function in reconstruction space will be discussed briefly. If the geometry is not known accurately, for example due to the complex nature of the detection system or due to its small size in combination with large manufacturing tolerances, it may be possible to measure the geometric function in reconstruction space. A technique in which a narrow light source is moved around in the reconstruction region has been applied regularly in the past.[4–6] This technique is not always applicable, for example when no narrow source is available in the right wavelength range (in the case of soft x-rays) or of a sufficient light strength (in the case of bolometers). If a parallel laser beam is available of the right strength and in the right wavelength region, a quantity here called angular étendue can be determined from measurements. This measurement technique is discussed and applied (Sec. 4) and it is shown that the geometric function in reconstruction space can be approximately calculated from the angular étendue.

The geometric function in reconstruction space is the most convenient way to characterize the detection system for tomography methods of the series-expansion type, i.e. methods in which the problem is discretized by expanding the local emissivity on a set of basis functions (for example pixels). The angular étendue, or the closely related geometric function in projection space (introduced later), is the most convenient quantity in some transform tomography methods.[7] Several examples of how the beam widths can be taken into account in tomographic reconstruction algorithms and the results of doing so have been published elsewhere.[8–10] Here, an example is given of deconvolution with the angular étendue to determine the peakedness of divertor radiation with much higher spatial resolution than achieved before (Sec. 5).

2. THE JET DIVERTOR BOLOMETER SYSTEMS

The bolometers used for the results in this paper have thin metal-film resistors and blackened gold absorber foils,[11] and are sensitive to radiation in the range visible to soft x rays (the main plasma radiation is in the vacuum uv region). Four bolometer channels are placed on one substrate and form one bolometer head. In contrast to Ref. 11, where a Kapton substrate is used, for JET a version with a mica substrate was developed.[12] The mica bolometers do not need to be cooled and have for several years been operated at 320ºC, which is the temperature at which the vacuum vessel is kept. The bolometers can be calibrated *in situ*,[11] i.e. without a calibrated light source, by heating the bolometer by passing a known current through the signal resistors and measuring the response. The calibration for the measurements described in Sec. 4 was carried out at room temperature in air, the calibration for the measurements of Sec. 5 was done in vacuum with the vessel at its normal temperature. A more detailed description of the complete bolometer systems in use on JET is given in Ref. 12.

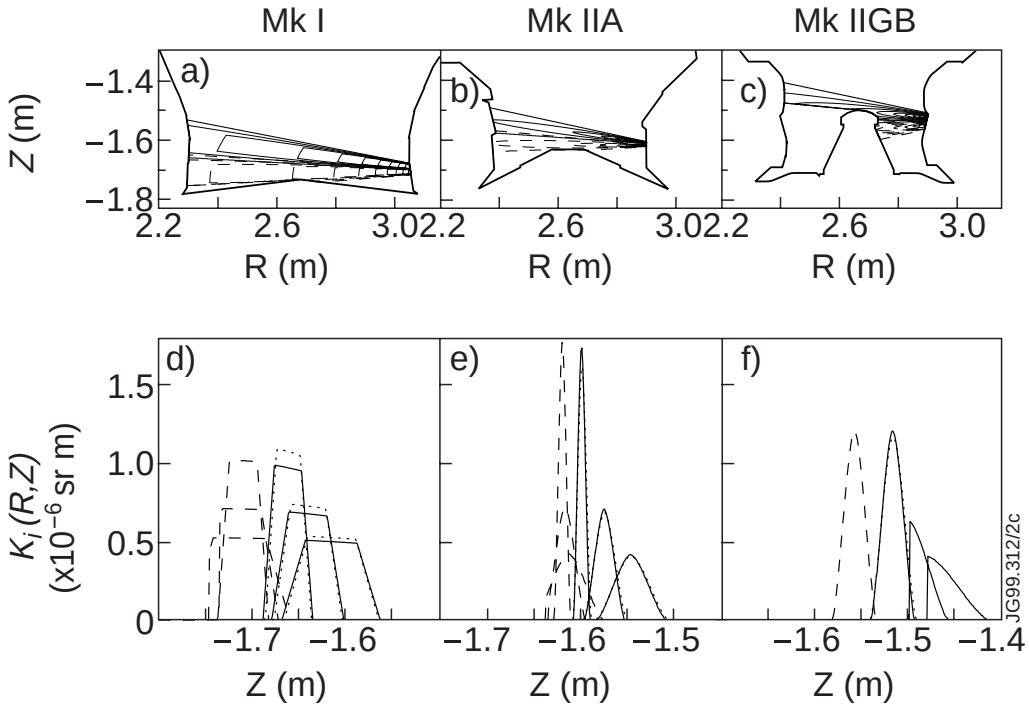

Fig.1: Illustration of the geometric function in reconstruction space $K_i(x = R, y = Z)$ *in poloidal coordinates* R *(major radius) and* Z *(height above midplane) for the three types of JET divertor bolometers of Fig.2. (a–c) Contour plots. The geometric functions of two bolometer channels are given, one with solid curves and one with dashed curves. The shape of the divertor tiles, which define the boundary of the reconstruction region in the divertor, is also shown. (d–f) Cross sections at major radii* $R = 2.45$ m, $R = 2.65$ m *and* $R = 2.85$ m. *All results were obtained numerically from Eq. (4), except the dotted curves in (a–c) for one of the detectors, which are obtained from Eq. (10).*

This paper is mainly concerned with the geometrical properties of detection systems. The JET bolometer systems in the divertor region form a good illustration of various types of geometry. The JET divertor is situated at the bottom of the vacuum vessel [see Figs.1(a)–1(c)]. In a fusion reactor the divertor will serve to divert from the bulk plasma and absorb part of the generated power. In JET and other tokamaks the performance of various divertor configurations is investigated.[13] For this purpose three different divertor configurations have been installed successively in JET since 1992, known as MkI, MkIIA and MkIIGB [see Figs.1(a)–1(c)], which range in geometric closure from open to closed. Due to the space restrictions and different regions of interest in the varying configurations, the bolometers had to be changed in each of the configurations. The bolometers are positioned in (or close to) one poloidal cross section of the tokamak (corresponding to the reconstruction plane), and usually the plasma emission can be assumed to be toroidally symmetric (the toroidal direction is perpendicular to the poloidal reconstruction plane). In MkI there was relatively much space and conventional pin-hole cameras could be used (the four bolometer channels of each bolometer head share one aperture), see Fig.2(a). Note that both the detector and aperture are rectangular. In MkIIA and MkIIGB the space restrictions were much more stringent, and the only option was to use individual collimators in front of each bolometer channels [Figs.2(b) and 2(c)]. Circular collimators were made with a

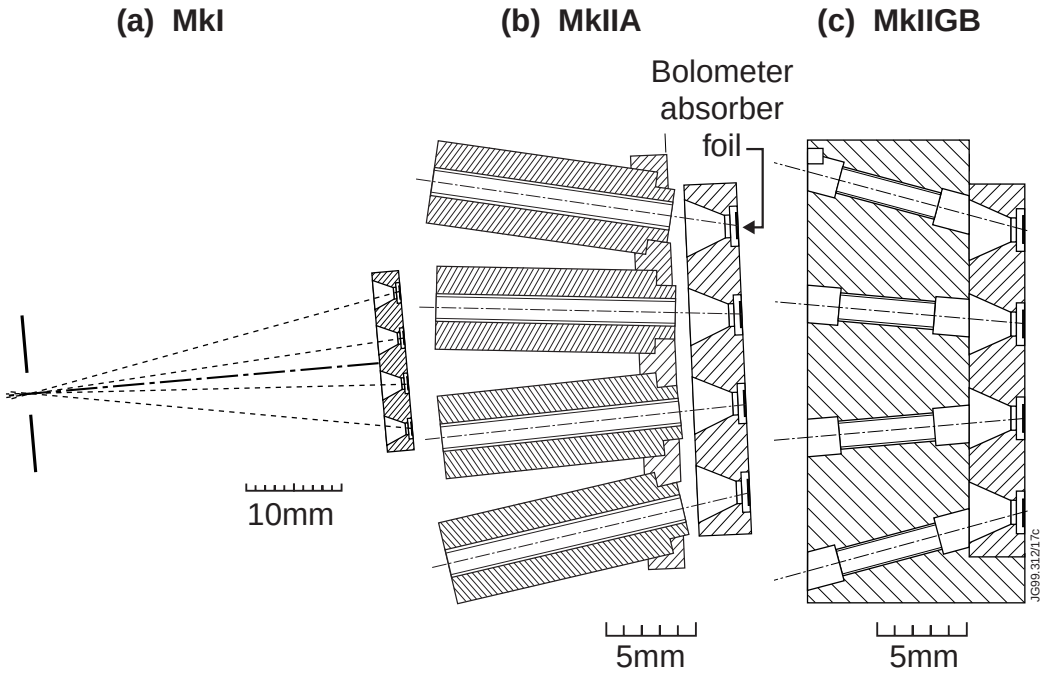

Fig.2: (a–c) Poloidal cross-section of three generations of divertor bolometer systems in JET (MkI, MkIIA and MkIIGB); each bolometer head consists of four channels. The collimators in (b) are double: one shifted perpendicular to the cross-section drawn.

thread that reduces reflections on the collimator walls (tests with visible light on collimators with blackened straight walls showed a significant effect of reflections; due to the grazing incidence of the light, reflections can also be expected to be significant in the uv). In MkIIA two identical collimators were stacked in the toroidal direction [out of the plane in Fig.2(b)], whereas in MkIIGB some of the bolometer heads were replaced with heads with single collimators in front of each channel. In one instance (not discussed further in this paper) it was even necessary to rotate the bolometer head so that the channels lay on one line in the toroidal direction and the collimators were tilted in both the poloidal and toroidal directions. Due to the small size of the collimators and the closeness of the collimators to the bolometer foils, the geometrical properties are very sensitive to misalignments and deviations from the design dimensions. In fact, the manufacturing tolerances were larger than could be accepted and therefore measurements were needed of the actual geometrical properties. These measurements are discussed in Sec. 4.

In the divertor chamber tiles are installed that should absorb the heat loads flowing to them from the plasma. In the toroidal direction there are gaps between tiles to make it possible for diagnostics to view the plasma and to allow for thermal expansion of the tiles. For some of the bolometer channels the tiles bound the viewing cone in the toroidal direction and have to be taken into account as (temperature dependent) additional apertures. Unfortunately, the laboratory measurements of Sec. 4 only give the geometrical properties of the bolometer head; the tile gaps have to be accounted for separately. These complications are outside the scope of this paper. Suffice it to say that in the geometric properties used in Sec. 5 the tile gaps have properly been taken into account.

3. CHARACTERIZATION OF GEOMETRIC PROPERTIES

The non-ideal measurement $\hat{f}_i$ by a detector *i* of a two-dimensional tomography system of a function $g(x,y)$ is given by

$$\hat{f}_i = \int_{-\infty}^{\infty}\int_{-\infty}^{\infty} K_i(x,y)\, g(x,y)\, \mathrm{d}x\, \mathrm{d}y, \tag{1}$$

where $K_i(x,y)$ is the geometric function in reconstruction space (*xy* space). In the case of emission tomography $g(x,y)$ is the local emissivity (units $\mathrm{Wm^{-3}sr^{-1}}$; $\hat{f}_i$ is in W); it is assumed that $g(x,y)$ is bounded and does not vary as a function of *z*, the third coordinate perpendicular to the *xy* plane. The geometric function $K_i(x,y)$ is the solid angle spanned by the entrance pupil of the detection system as seen from point (x,y), integrated over the third dimension, and can be calculated accordingly. Ideal measurements are given by the Radon transform of the function $g(x,y)$:

$$f(p,\xi) = \int_{-\infty}^{\infty}\int_{-\infty}^{\infty} \delta(p + x\sin\xi - y\cos\xi)\, g(x,y)\, \mathrm{d}x\, \mathrm{d}y, \tag{2}$$

where *p* is the signed distance between the line and the origin, and ξ is the angle of the line with the positive *x* axis (note that some authors use a definition for the angle that is different by $\pi/2$). The parameters of a line (p,ξ) are coordinates of a space called projection space. The range of the ξ coordinate is usually chosen as $[0\ldots\pi]$ (the property $f(p,\xi+\pi) = f(-p,\xi)$ applies), but in some graphs where ξ is close to π, we extend the range beyond π. Under certain conditions the non-deal measurement $\hat{f}_i$ can be approximated by the ideal line integral value $f(p_i,\xi_i)$ (units $\mathrm{Wm^{-2}sr^{-1}}$), where (p_i,ξ_i) are the projection-space coordinates of the average line of sight. In that case the approximate kernel in Eq. (1) is given by $K_i(x,y) = E_i\,\delta(p_i + x\sin\xi_i - y\cos\xi_i)$, where E_i is the étendue of the detection system (units $\mathrm{srm^2}$). The quantity here called étendue is often given the name "throughput", or many other names (for a discussion on terminology see Ref. 14 and references therein). See Ref. 10 for a discussion on the applicability of the line-integral approximation; in this paper we consider detection systems for which this approximation is inappropriate.

In projection space Eq. (1) can be stated as[10]

$$\hat{f}_i = \int_0^{\pi}\int_{-\infty}^{\infty} k_i(p,\xi)\, f(p,\xi)\, \mathrm{d}p\, \mathrm{d}\xi,$$

where $k_i(p,\xi)$ is the geometric function in projection space. The geometric function in projection space can be calculated by[10]

$$k_i(p,\xi) = \int_{-\infty}^{\infty}\int_{-\pi/2}^{\pi/2} \eta_i(p,\xi,z,\theta)\cos\theta\, \mathrm{d}\theta\, \mathrm{d}z, \tag{3}$$

where η_i is a filter function for rays, which is the attenuation of the ray, or zero if this ray does not go through the entrance pupil of the detection system for detector *i* from the right direction. The ray can be described completely by four parameters, for which we choose *p*, ξ, *z* and θ.

Here, z is the height where the line intersects a reference plane (for instance the detector), and θ is the angle of the line with respect to the xy plane. It is not trivial that $k_i(p,\xi)$ can describe the geometric properties of the detection system in the third dimension; that this is possible is related to the conservation of the étendue through optical detection systems.[10] Some ideas of the coverage of projection space by a function similar to $k_i(p,\xi)$ have been described in the past by Beattie[15] and Lindgren and Rattey,[1] and a relationship similar to Eq. (4) below (and an equivalent statement to the conservation of the étendue) has been given for transmission tomography by Verly,[16] but we are not aware of a similar consistent application to projection space as in Ref. 10. The geometric function in projection space $k_i(p,\xi)$ can be expressed analytically if the detector and the (single) aperture of the detection system are rectangular (see Appendix A).

Although it is easy to express $K_i(x,y)$ in terms of the filter function η_i and to calculate it numerically by integrating over z, ξ and θ, it can be more efficient to first calculate $k_i(p,\xi)$ and then $K_i(x,y)$ from[10]

$$K_i(x,y) = \int_0^{\pi} \int_{-\infty}^{\infty} k_i(p,\xi)\,\delta(p + x\sin\xi - y\cos\xi)\,\mathrm{d}p\,\mathrm{d}\xi. \tag{4}$$

The reason for this is that with the effectively one-dimensional integral (4) one makes use of the property that $k_i(p,\xi)$ is the same on all points (x,y) on the line $p = -x\sin\xi + y\cos\xi$ [i.e. $k_i(p,\xi)$ is a function of (p,ξ) only], whereas the straightforward calculation of $K_i(x,y)$ has three independent integrals. If an analytical expression of $k_i(p,\xi)$ is available, the calculation of $K_i(x,y)$ is very fast. Although the inverse of Eq. (4) can be described formally,[10] no satisfactory numerical method has been found so far to calculate $k_i(p,\xi)$ from $K_i(x,y)$.

The effective size of the entrance pupil seen by a parallel beam of light at angles ξ and θ is

$$t_i(\xi,\theta) = \int_{-\infty}^{\infty} \int_{-\infty}^{\infty} \eta_i(p,\xi,z,\theta)\cos\theta\,\mathrm{d}p\,\mathrm{d}z,$$

where the $\cos\theta\,\mathrm{d}z$ term reflects the size of element dz perpendicular to the beam of light (note that p is already defined perpendicular to the beam). We will refer to $t_i(\xi,\theta)$ as transmission function.

If the size of the detector or apertures in the reconstruction plane are small with respect to the reconstruction region and the structures in the reconstruction region that should be resolved, a good and useful approximation of the function $k_i(p,\xi)$ is the angular étendue

$$e_i(\xi) = \int_{-\infty}^{\infty} k_i(p,\xi)\,\mathrm{d}p, \tag{5}$$

or equivalently

$$e_i(\xi) = \int_{-\pi/2}^{\pi/2} t_i(\xi,\theta)\,\mathrm{d}\theta. \tag{6}$$

The name of the angular étendue stems from the fact that it gives the angular dependence of the integrand that yields the étendue[10]

$$E_i = \int_0^{\pi} \frac{e_i(\xi)}{\cos(\xi - \xi_i)} \mathrm{d}\xi. \tag{7}$$

The angular étendue can be visualized as being $k_i(p,\xi)$ compressed onto a curve in projection space, called aperture curve, that corresponds to the lines of sight through a characteristic point of the detection system, for example the center of the most bounding aperture or the detector. The approximation of $k_i^L(p,\xi)$ in terms of the angular étendue is therefore given by

$$k_i(p,\xi) \approx k_i^L(p,\xi) = e_i(\xi)\,\delta(p - p_{\mathrm{ap}}(\xi)), \tag{8}$$

where $p_{\mathrm{ap}}(\xi) = -x_{\mathrm{ap}} \sin\xi + y_{\mathrm{ap}} \cos\xi$ is the aperture curve defined by the coordinates $(x_{\mathrm{ap}}, y_{\mathrm{ap}})$ of the characteristic point. Substituting Eq. (8) into (4) gives

$$K_i(x,y) \approx K_i^L(x,y) = \int_0^{\pi} e_i(\xi)\,\delta(p_{\mathrm{ap}}(\xi) + x\sin\xi - y\cos\xi)\,\mathrm{d}\xi, \tag{9}$$

i.e. the function $K_i^L(x,y)$ describes the fan of line integrals of lines through $(x_{\mathrm{ap}}, y_{\mathrm{ap}})$ weighted by $e_i(\xi)$.

Figures 1 and 3 illustrate the quantities introduced above as calculated using the design geometry for pairs of adjacent bolometer channels in the three different JET divertors MkI, MkIIA and MkIIGB. The quantities for the MkI bolometers in Fig. 3(a–c) were calculated with the analytical formulae of Appendix A, whereas the integrand of the integrals for the other bolometers was evaluated numerically with ray tracing. The contours in Fig. 3(a) are vertical because the aperture and detector are parallel (see Appendix A), whereas in Figs. 3(b) and 3(c) the contours are curved due to several circular apertures. Integrating the contour plots of Figs. 3(a)–3(c) over p, i.e. Eq. (5), and Fig. 3(d)–3(f) over θ, i.e. Eq. (6), gives the same result (within numerical accuracy) for the angular étendue [Fig.3(g)–3(i)]. The quantity $k_i(p,\xi)$ is more useful in practice than $t_i(\xi,\theta)$ because $k_i(p,\xi)$ has all relevant information about the third dimension compressed into it [the values of $k_i(p,\xi)$] and contains all geometrical information about the reconstruction plane [the region where $k_i(p,\xi)$ is non-zero]. Therefore, $k_i(p,\xi)$ can be used directly in tomography algorithms or indirectly to calculate $K_i(x,y)$. In contrast, $t_i(\xi,\theta)$ scrambles information about the third dimension and the reconstruction plane, and has no direct application in tomography algorithms, but only an indirect application because it is a measurable quantity.

From the quantities in Fig.3 the geometric function in reconstruction space can be calculated. Contour plots and cross sections of this function are shown in Fig.1. The geometric functions in reconstruction space displayed as solid and dashed lines in Fig.1 were calculated numerically with Eq. (4). Note that, because the shape of the divertor is not convex, some

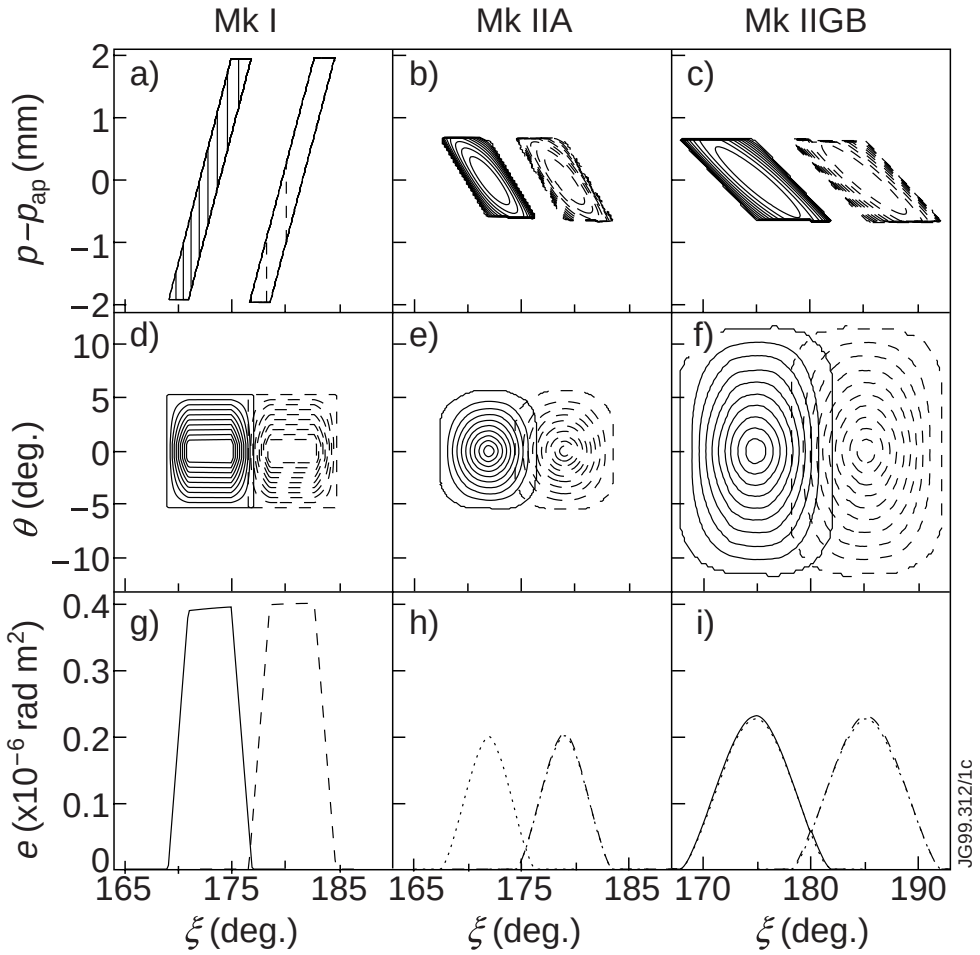

Fig.3: Illustration of (a–c) $k_i(p-p_{\mathrm{ap}},\xi)$, (d–f) $t_i(\xi,\theta)$ (both as contour plots) and (g–i) e(ξ) for the three types of JET divertor bolometers of Fig.2; tile gaps that limit the view of some detectors in the toroidal direction were not taken into account. The functions are given for two detectors, one indicated by solid curves and one by dashed curves. The solid and dashed curves in (h–i) were obtained from $k_i(p,\xi)$ [Eq. (5)], the dotted curves from $t_i(\xi,\theta)$ [Eq. (6)]. Contour levels in (a) are separated by 0.3% of the maximum value, whereas the contours in the other graphs are at 10%. Note that $k_i(p-p_{\mathrm{ap}},\xi)$ are plotted with respect to the aperture curve.

structures obstruct the view of some channels. The representation in projection space, in the form presented here, is not suitable if the reconstruction region is not convex (see Ref. 17 for a more complete treatment). This is only a minor problem in the present application: Eq. (4) has to be extended to chop off the geometric function in reconstruction space if the light path is obstructed. The approximation $K_i^L(x,y)$ with Eq. (9) gives a very similar result [dotted cross sections in Fig.1(d)–1(f)]; as one can expect the function is slightly narrower (by the width of the aperture or the detector), and a bit higher so that the integral over the cross-section is the same as the exact geometric function; this integral is equal to the étendue.[10] Although the approximation with $K_i^L(x,y)$ seems straightforward, its calculation is not. The problem is that the line integrals, given by the delta function of Eq. (9), need to be calculated and averaged over a finite space (for example a pixel) and then be assigned to a single point. If a pixel centered at (x_j,y_j) is given by the function $b(x-x_j,y-y_j)$, which is 1 inside the pixel and 0 outside, then

its Radon transform [Eq. (2)] $L(p,\xi,x_j,y_j)$ is the length through the pixel. In these terms, the average of $K_i^L(x,y)$ over the pixel is given by

$$\overline{K}_i^L(x_j,y_j) = \int_0^\pi e_i(\xi)\, L(p_{\mathrm{ap}}(\xi),\xi,x_j,y_j)\, \mathrm{d}\xi. \tag{10}$$

This equation is also valid if more advanced basis functions than pixels are used. To achieve the same accuracy as can be obtained with Eq. (4), actually more computation time is needed due to the average over a finite region. However, if the accuracy is of less importance, it may well be that Eq. (10) is easier to implement in existing tomography algorithms that assume the measurements to be along infinitely thin lines [the weighted integral of Eq. (10) is over a set of such lines], instead of implementing the full geometric function averaged over the basis functions.

4. MEASUREMENT OF APPROXIMATE GEOMETRIC FUNCTION IN PROJECTION SPACE

To measure the geometric function in reconstruction space a long thin light source is needed; its length must cover the maximum extent of the views in the direction perpendicular to the reconstruction region (toroidal bending is neglected). Long thin light sources can take different forms, for instance a tube light,[6] or a tall thin beaker filled with a scattering medium (milk dissolved in water) and a flashlight as light source.[4] The light source is moved around in the entire reconstruction region in a regular pattern (in practice over a thousand points) and the response of all detectors is measured. The light source in position (x_j,y_j) is considered to be a delta function $g(x,y) = I_0\, \delta(x-x_j)\, \delta(y-y_j)$, and each measured amplitude therefore [Eq. (1)] directly gives the geometric function in reconstruction space (after scaling with the calibration factor I_0). Of course the finite size of the light source will result in some blurring of the geometric function, but if the light source is sufficiently thin, i.e. much smaller than the structures to be resolved by tomography, this is negligible.

As discussed in the Introduction, such a direct measurement of the geometric function is not always possible, for example when no sufficiently powerful long thing light source is available in the spectral region of interest. In such a case it may be possible to measure $t_i(\xi,\theta)$ directly. We took such measurements by shining a parallel laser beam onto the bolometer assembly at many different angles ξ and θ. A standard 8-mW HeNe laser with a commercial 20× beam expander was sufficient for the required degree of accuracy. The laser beam has to be expanded sufficiently to be approximately uniform across the detector (we achieved a uniformity within 5%) and should be absolutely calibrated (we had to adjust the calibration factor of a poor absolute calibration to obtain the best average fit to all channels). Figure 4 shows a series of measurements of $t_i(\xi,\theta)$ for four neighboring channels of one of the MkIIGB bolometer systems (θ=0°) and for comparison the calculated values using the design values of the geometry. There are some differences between the measurements and calculations. The differences in height and width are

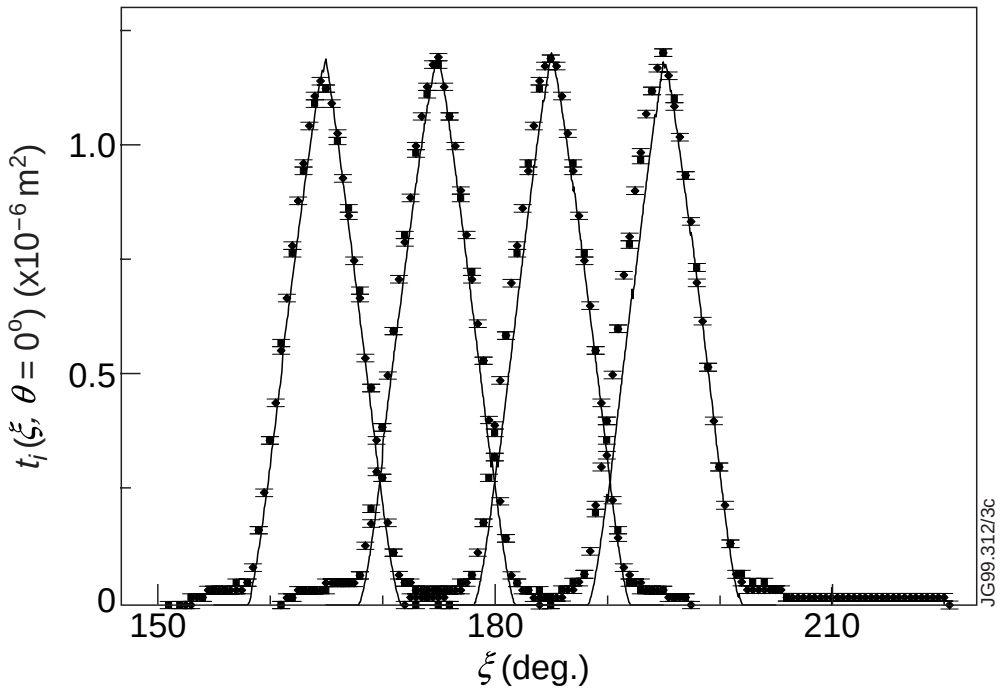

Fig.4: Measured (points) and calculated (line) cross section $t_i(\xi, \theta = 0°)$ for one of the MkIIGB bolometer heads with four channels. The diamonds and squares indicate two measurement series.

likely to be caused by variations in the toroidal angle, variations in collimator length and collimator diameter, i.e. the actual values deviate from the design values, and by reflections on the threaded wall of the aperture. The pedestal at the edges are also likely to be caused by reflections; in blackened non-threaded collimators these reflections were found to be at least one order of magnitude worse. From these and more measurements (at different θ) the angular étendue can be calculated with Eq.(6) and then the geometric function in reconstruction space can be approximated with Eq. (10).

5. DECONVOLUTION OF BEAM-WIDTH EFFECTS

Instead of showing the relevance of the beam widths and how they are taken into account in tomography methods, all of which has been published elsewhere,[8–10] here an illustration is given of how the angular étendue can be used to approximately reconstruct the ideal measurements from non-ideal measurements that were blurred by the beam widths. Such a reconstruction is only possible if the separation between the average lines-of-sight of adjacent measurements is much smaller than the beam widths; in other words: the spatial sampling frequency must be much higher than the width of the Fourier transform of the instrument function,[3,18] otherwise insufficient information is available to retrieve the ideal values. In most detection systems for tomography this condition is not met: the sampling and beam widths are matched such that the beams of adjacent channels do not overlap or overlap up to halfway (see Figs.1 and 3 for examples); note that if there are high spatial frequencies in the function $g(x,y)$, this can lead to considerable aliasing.[18] In some instances many more virtual lines of sight can be created by

taking into account movement of the object under consideration, in our case the tokamak plasma. In the past such a method has regularly been applied with plasma rotation.[19] Deliberate linear movements of the plasma have also been used to gain more information about the extent of blurring,[20] and to resolve more details in the tomographic reconstruction.[21] We show that useful information about the localization of plasma emission can be obtained by deconvolution of non-ideal measurements of adjacent channels during movement of the plasma.

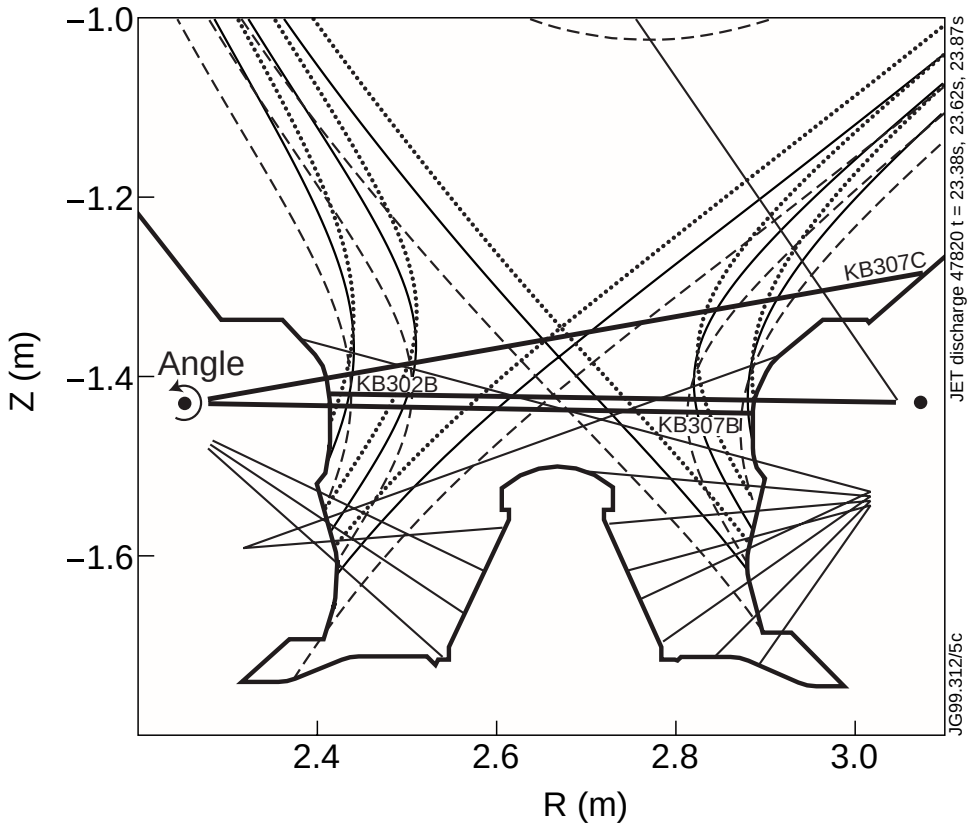

Fig.5: Magnetic flux surfaces (solid, dotted and dashed curves) during various stages of the sweep. Thick solid lines: the three bolometer lines of sight analyzed; thin lines: other divertor bolometer channels. The outline of the divertor tiles is shown and the angle used to map the sweep to virtual lines of sight is indicated.

In our experiment the entire plasma was swept up and down with respect to the horizontal bolometer divertor channels (see Fig.5), without a significant change of plasma conditions. We consider three channels that view the plasma near the so called X-point (i.e. where the magnetic configuration of the bulk plasma and divertor plasma are separated, see Fig.5), a region where at high plasma densities the divertor radiation peaks and where therefore knowing the detailed radiation profile is of particular interest. We consider L-mode plasmas with about 2 MW of non-Ohmic heating close to the density limit (line-averaged density $\bar{n}_e > 3.4 \times 10^{19}\,\mathrm{m}^{-3}$). The vertical movement of the plasma can be mapped to the angle around the intersection of the two lines of sight (called KB307B and KB307C) that view the plasma from the left (this angle is indicated in Fig.5), thus the measurements in time can be mapped to this angle [Fig.6(a)]. Because of symmetry, also the measurements of the channel on the right (channel KB302B) can be approximately

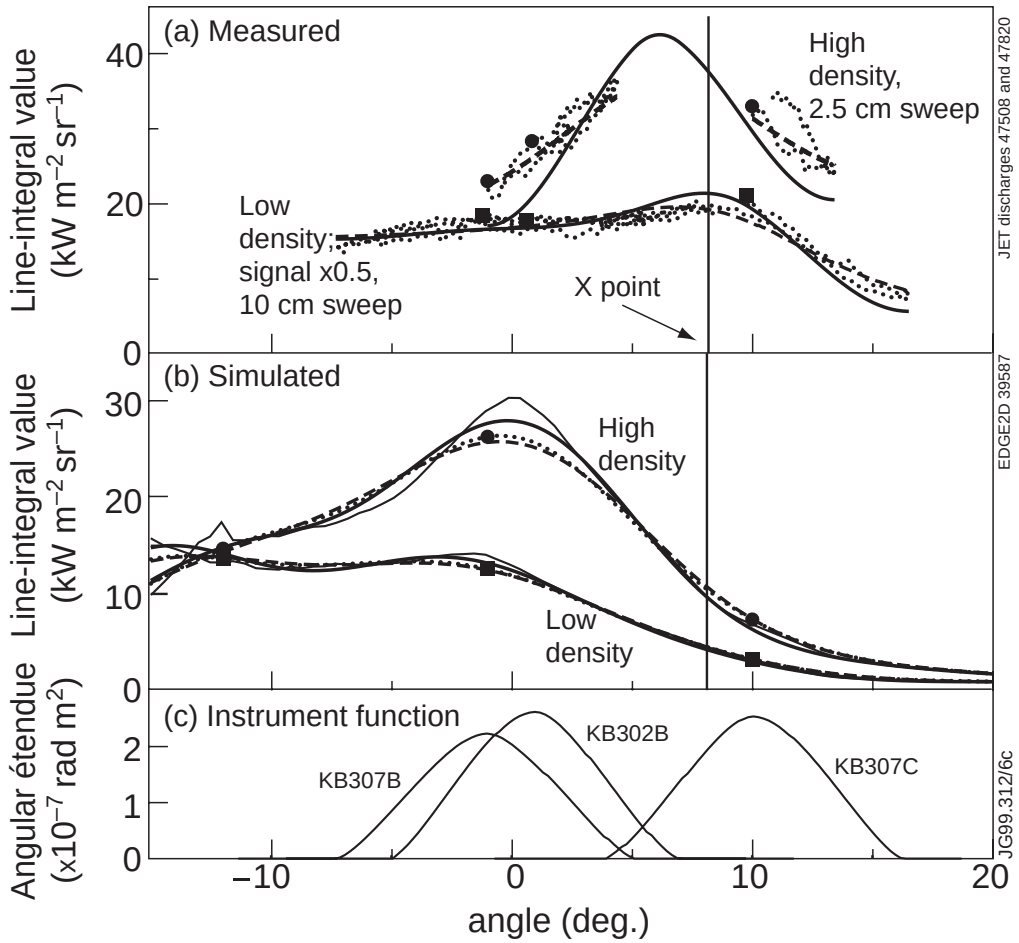

Fig.6: Reconstruction of line-integral values from non-ideal bolometer measurements during X-point sweeps in high-density plasmas. (a) Experimental data during a lower density plasma (line-averaged density $\bar{n}_e \approx 3.1\times10^{19}\,m^{-3}$*, 10 cm sweep, signal divided by 2) and a high-density plasma close to the density limit (*$\bar{n}_e \approx 3.4\times10^{19}\,m^{-3}$*, 2.5 cm sweep) in the MkIIGB divertor. (b) Data for a low (*$\bar{n}_e = 1.5\times10^{19}\,m^{-3}$*) and high-density (*$\bar{n}_e \approx 3.0\times10^{19}\,m^{-3}$*) plasma from a plasma transport simulation of a similar plasma in the MkIIA divertor (also with vertical targets). (c) Instrument functions (angular étendues) of the three bolometer channels considered. The non-ideal measurements in (a,b) have been scaled to the étendue:* $\hat{f}_i(\xi(t))/E_i$*. The points indicate the information that would have been available without the sweep. The thin solid curve in (b) shows the pure line-integral values (to be reproduced as well as possible by the reconstruction). The dotted curves in (a) and (b) give the non-ideal measurements (mapped to angle). Thick solid curves are the reconstructed values, and the thick dashed curves are backcalculated values from the reconstruction.*

mapped to this angle. The measurements in Fig.6(a) have been scaled by the étendue to a line-integral value, so that the three channels with somewhat different étendues can be compared. The reasonable overlap between the various measurements during upward and downward sweep is an indication that indeed the plasma conditions did not change much during the sweep. The reasonable overlap between channels KB302B and KB307B indicates that the approximation of mapping them to the same angle is reasonable. The angular étendue is approximately the instrument function by which pure line-integral measurements are blurred. If one can assume that, apart from a scaling by the étendue, the angular étendues of the three channels are approximately the same [Fig.6(c)], the measurements as a function of angle ξ are given by

$$\hat{f}(\xi) = \int_0^{\pi} e(\xi' - \xi) \;\; f(\xi') \;\; \mathrm{d}\xi' . \qquad (11)$$

If $e(\xi)$ is symmetric, Eq. (11) is a convolution in the strict mathematical sense, and a deconvolution of the non-ideal measurement $\hat{f}(\xi)$ [dotted curves in Fig.6(a)] can give an approximation of the ideal values $f(\xi)$. For the solution method ("deconvolution") used here, Eq. (11) is inverted and the requirement that $e(\xi)$ be symmetric is not needed. We used a standard regularized inversion technique to obtain the smoothest solution that is consistent with the measurements (Appendix B). The resulting reconstruction is also shown in Fig.6(a) (solid line), and furthermore the reconstructed values inserted into Eq. (11) ("backcalculation"; dashed curves) which should be a fit to the measurements. It is clear that a reasonable reconstruction has been obtained that demonstrates detail of the peak in the radiation close to the X point, and that substantially more information has been obtained from the sweep experiment than would have been available without the sweep [the points in Fig.6(a)].

The same kind of calculations have been performed on the results of two-dimensional plasma-transport simulations of a similar JET discharge [Fig.6(b)]. The simulations were done with the EDGE2D/NIMBUS code and are described in more detail in Ref. 9. From the simulation results it was calculated what the bolometers would measure if the simulated emission profile were actual, both with ideal measurements (thin solid line) and non-ideal measurements (dotted line). In this case the reconstructed values [thick solid curve in Fig.6(b)] show that the blurring of the convolution can indeed be partly reversed by the reconstruction method, but that due to the finite measurement errors the peak values are underestimated. It should be noted that with the smoothness assumption, of all possible solutions of Eq. (11), the present reconstruction method obtains the smoothest solution. This means that in reality more structure may be present in the emission profile (which cannot be obtained from the measurements without further knowledge), but not less. Therefore, the value of the present reconstructions is that they show the minimum peakedness that is consistent with the measurements.

From the reconstructions in Fig.6 it follows that at very high plasma density the line-integrated emission profile as a function of angle is rather peaked just below the X point, both in the measured and simulated data. The local emissivity (i.e. not line integrated) can be expected to be considerably more peaked still in the vertical direction. This detailed information is important, because it contrasts with what is found in high-density impurity-seeded H-mode plasmas, where there are indications (from low-resolution unswept measurements) that the radiating peak is above the X point (inside or outside the separatrix). Unfortunately, no such detailed information can be derived in the horizontal direction as the plasma cannot be swept in that direction in the gas-box divertor and because the instrument functions of channels looking vertically are considerably wider than those of the divertor channels. It is not completely understood why the experimental lower plasma density case [Fig.6(a)] radiates as much as the high-density case; however, the measurements are from two discharges and there are differences

between the two discharges in the amount of input power, in the way the high plasma density is reached and in the ratio of impurity radiation to deuterium radiation. It is also not understood why the radiating peak is higher in the measurements (in MkIIGB) than in the simulations (in MkIIA; simulations are in good correspondence with the measurements in MkIIA[9]).

6. SUMMARY

Several methods to describe, calculate and measure the geometrical properties of detection systems for two-dimensional tomography have been discussed. This paper considers emission tomography only, but many of the concepts discussed can probably be used in transmission tomography as well. Although some quantities introduced in Sec. 3 to describe the geometric properties of a detection system are abstract, all quantities of that section are useful. The geometric function in reconstruction space can be used directly in series-expansion tomography methods (after integration over the basis functions, such as square pixels) to take into account the beam-width effects.[10] The geometric function in projection space can be a useful quantity to take into account the beam-width effects in certain tomography methods that operate in projection space (such as the Cormack and Iterative Projection-space Reconstruction methods).[7] The angular étendue is a convenient approximation for this purpose. The geometric function in projection space also gives efficient means to calculate the geometric function in reconstruction space; this is also possible from the angular étendue, but on that route one encounters numerical limitations. If the reconstruction region is not convex (i.e. a part of the viewing beam is blocked by an external structure that cannot be taken into account in the geometric function in projection space), an additional check in Eq. (4) is needed to determine whether the point (x,y) is actually seen by the detector. The étendue of the detection system is required if one wishes to approximate the measurements by line integrals [Eq. (2)]. In Sec. 4 it was shown that the transmission is a directly measurable quantity, from which the angular étendue and approximations of the geometric function and the étendue can be derived. Finally, the angular étendue can be used to approximately reconstruct ideal measurements from non-ideal measurements that were blurred by the beam widths. In the divertor of the JET tokamak this method gives useful information on the extent of the radiating peak near the X point in high-density divertor plasmas.

ACKNOWLEDGMENTS

We gratefully acknowledge the technical support of S. Dillon and D.J. Wilson in the design of the bolometer systems, and the support of P. Beaumont and P.J. Böcker in the measurements and calculations of the geometrical properties. We also thank the members of the JET Task Force for ELMy H-mode Physics for carrying out the X-point sweep experiments.

APPENDIX A: SOME GEOMETRIC PROPERTIES OF PIN-HOLE CAMERAS

The description in projection space of a simple pin-hole system with rectangular detector and rectangular aperture is straightforward and several quantities can be expressed analytically. These expressions are valuable because such detection systems are regularly applied in practice.

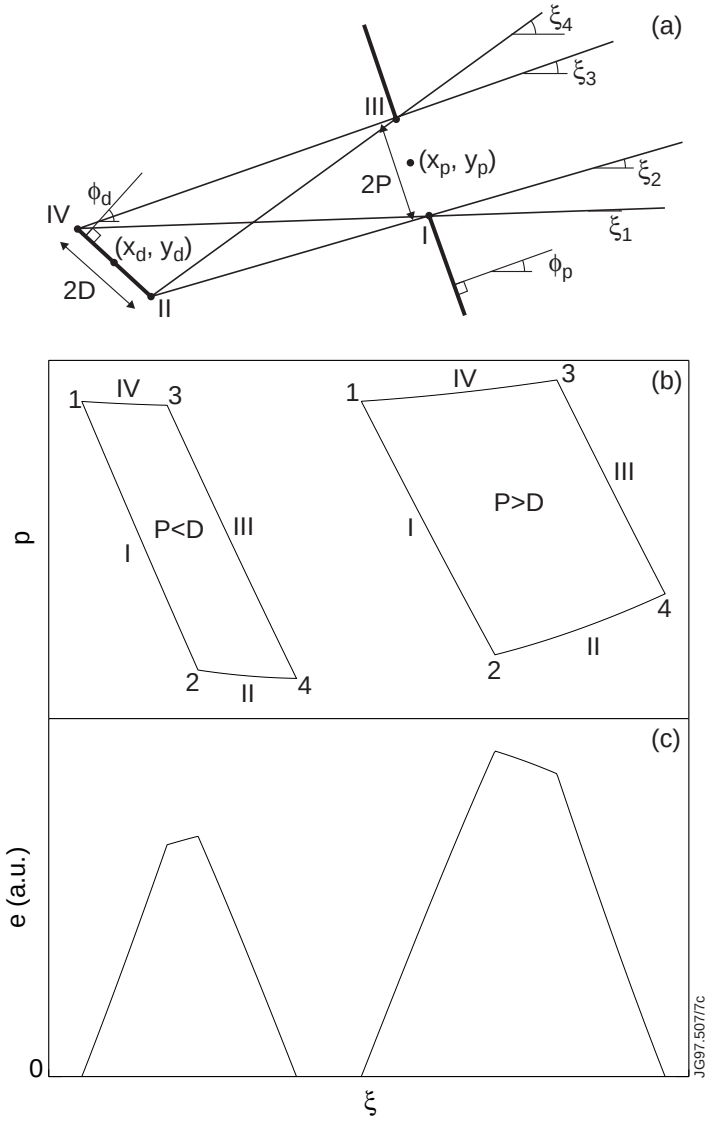

Fig.7: (a) Geometry in the xy *plane of the pin-hole system discussed in Appendix A. (b) Boundaries in projection space for two pin-hole systems with varying pinhole size. The detector and aperture were taken parallel. The angles at which the curves start and end are given in Table I. (c) Angular étendues for the systems of (b).*

The geometry of the pin-hole system under consideration is shown in Fig.7(a). It is assumed that the detector and aperture are rectangular and have two edges parallel to the *xy* plane, and that the detector and aperture are perpendicular to the *xy* plane. The boundaries of the region covered in projection space are shown in Fig.7(b). Two cases are considered: one where the aperture is larger than the detector and vice versa (the effective sizes if the detector and aperture are not parallel). The coordinates of the bounding points I to IV and the angles are given in Table I. The functions of the boundary curves in Fig.7(b) are

$$p_h(\xi) = -x_h \sin\xi + y_h \cos\xi, \tag{12}$$

where h is I … IV. The width of the region in the p direction is related to the aperture size.

Table I. *Bounding points and angles of the pin-hole system shown in Fig.7.*

Point h	x_h	y_h	ξ range	Angle ε	$\tan\xi_\varepsilon$
I	$x_p + P \sin\phi_p$	$y_p - P\cos\phi_p$	$\xi_1 \rightarrow \xi_2$	1	$(y_I - y_{IV})/(x_1 - x_{IV})$
II	$x_d + D \sin\phi_d$	$y_d - D\cos\phi_d$	$\xi_2 \rightarrow \xi_4$	2	$(y_I - y_{II})/(x_1 - x_{II})$
III	$x_p + P \sin\phi_p$	$y_p - P\cos\phi_p$	$\xi_4 \rightarrow \xi_3$	3	$(y_{III} - y_{IV})/(x_{III} - x_{IV})$
IV	$x_d + D \sin\phi_d$	$y_d - D\cos\phi_d$	$\xi_3 \rightarrow \xi_1$	4	$(y_{III} - y_{II})/(x_{III} - x_{II})$

If for a given line (p,ξ) the distance between the points of intersection on the detector and aperture is $L(p,\xi)$, and in the z direction the detector extends between z_d^- and z_d^+, and the aperture between z_p^- and z_p^+, one can calculate

$$\begin{aligned} k_i(p,\xi) &= \int_{z_d^-}^{z_d^+}\int_{\theta^-}^{\theta^+} \cos\theta \, d\theta \, dz \\ &= \sqrt{L^2(p,\xi) + (z_p^+ - z_d^-)^2} - \sqrt{L^2 + (z_p^- - z_d^-)^2} - \sqrt{L^2 + (z_p^+ - z_d^+)^2} + \sqrt{L^2 + (z_p^- - z_d^+)^2}, \end{aligned} \tag{13}$$

where the z integral is carried out over the detector surface [Eq. (3) shows that any z integral for constant (p,ξ) will give the same result, which is related to the conservation of the étendue] and it has been realized that the bounds of θ are given by $\sin\theta^\pm = (z_p^\pm - z)/\sqrt{L^2(p,\xi) + (z_p^\pm - z)^2}$.

If the detector and aperture are parallel, $L(p,\xi) = L(\xi)$ will be independent of p, and so will $k_i(p,\xi)$ from Eq. (13). Therefore, the angular étendue of Eq. (5) can be expressed analytically as

$$e_i(\xi) = k_i(\xi)\,\Delta p(\xi),$$

where $\Delta p(\xi)$ is the difference of the curves of Eq. (12) in the appropriate interval. The angular étendue of the detectors of Fig.7(b) is shown in Fig.7(c).

For parallel detector and aperture, the transmission function $t_i(\xi,\theta)$ can be expressed as $t_i(\xi,\theta) = t_{i,z}(\xi,\theta)\,\Delta p(\xi)$, with $t_{i,z}(\xi,\theta)$:

$$t_{i,z}(\xi,\theta) = \begin{cases} 0 & \text{for } \theta \le \theta_1 \text{ and } \theta \ge \theta_4 \\ (-(z_p^- - z_d^+) + L(\xi)\tan\theta)\cos\theta & \text{for } \theta_1 \le \theta \le \min(\theta_2,\theta_3) \\ (z_d^+ - z_d^-)\cos\theta & \text{for } \theta_2 \le \theta \le \theta_3 \text{ if } \theta_2 \le \theta_3 \\ (z_p^+ - z_p^-)\cos\theta & \text{for } \theta_3 \le \theta \le \theta_2 \text{ if } \theta_3 \le \theta_2 \\ ((z_p^+ - z_d^-) - L(\xi)\tan\theta)\cos\theta & \text{for } \max(\theta_2,\theta_3) \le \theta \le \theta_4 \end{cases}$$

where $\theta_1 = \arctan((z_\mathrm{p}^- - z_\mathrm{d}^+)/L(\xi))$, $\theta_2 = \arctan((z_\mathrm{p}^- - z_\mathrm{d}^-)/L(\xi))$, $\theta_3 = \arctan((z_\mathrm{p}^+ - z_\mathrm{d}^+)/L(\xi))$ and $\theta_4 = \arctan((z_\mathrm{p}^+ - z_\mathrm{d}^-)/L(\xi))$. Note that for parallel detector and aperture the integral of $t_{i,z}(\xi,\theta)$ over θ equals $k_i(\xi)$ [from Eq. (13)].

The integrand in Eq. (7) will be a complicated function in ξ, and the étendue can therefore probably only be calculated numerically. However, if the detector and aperture dimensions, *D* and *P*, are small compared to the perpendicular distance ℓ between the detector and aperture planes, a Taylor expansion in ξ around $\bar{\xi}_i$, and expansions making use of the smallness of *D* and *P* with respect to ℓ, give an expression consistent with the simple formula $E = A_\mathrm{eff}\Omega_\mathrm{eff}$, where A_eff and Ω_eff are the effective detector area and effective solid angle spanned by the aperture, respectively. For a simple pin hole with parallel detector and aperture the zeroth order term gives

$$E_i(\bar{\xi}_i) \approx \frac{A_\mathrm{d}A_\mathrm{p}}{\ell^2}\cos^4(\bar{\xi}_i - \phi_\mathrm{d}), \tag{14}$$

where A_d and A_p are the detector and aperture areas, respectively. Equation (13) is a well known approximation of the étendue.

With $k_i(p,\xi)$ from Eq. (13) the geometric function in reconstruction space can be calculated by Eq. (4). Again the integrand is rather complicated and may only be calculable numerically. If, however, the same approximations are valid as the ones that led to Eq. (13), $k_i(p,\xi) \approx k_0$ will be approximately constant and the geometric function in reconstruction space can be calculated analytically as $K_i(x,y) \approx k_0\Delta\xi_i(x,y)$, where $\Delta\xi_i(x,y)$ is the ξ distance between the points of intersection of the curve $p = -x\sin\xi + y\cos\xi$ with the boundary curves in Fig.7(b).

APPENDIX B: REGULARIZED INVERSION

Our aim is to invert Eq. (11), i.e. to obtain the ideal $f(\xi)$ from the non-ideal measured $\hat{f}(\xi)$. Many ways exist to approach this problem. It is important to realize that the problem is ill-posed, i.e. the inversion is extremely sensitive to noise and no unique solution exists. We have solved the problem with a so-called constrained optimization method, requiring the solution to be smooth, and using the discrepancy principle.[22] First, we discretize the problem to $\hat{\boldsymbol{f}} = A\boldsymbol{f}$, where $\hat{\boldsymbol{f}}$ and $\boldsymbol{f}$ are vectors of which the elements are $\hat{f}(\xi)$ and $f(\xi)$ at discrete angles ξ_m, and $A_{mn} = e(\xi_n - \xi_m)$. We intend to find the smoothest solution that fits the data. The unsmoothness can be expressed as a scalar in terms of the second derivative of *f*,

$$\langle f|\Omega|f\rangle = \int_0^\pi \left(\frac{\mathrm{d}^2 f(\xi)}{\mathrm{d}\xi^2}\right)^2 \mathrm{d}\xi,$$

where the brackets in Dirac notation designate the scalar product of functions or vectors. In

matrix form, $\Omega = D_{\xi\xi}^{\mathsf{T}} D_{\xi\xi}$, where $D_{\xi\xi}$ is the second derivative matrix.[23] Minimizing the unsmoothness with the constraint $\left\| \hat{\boldsymbol{f}} - A\boldsymbol{f} \right\| \leq \|\varepsilon\|$, where ε is the estimated measurement error, leads to the equation

$$\left(\lambda A^{\mathsf{T}} A + \Omega\right)\mathrm{f} = \lambda A^{\mathsf{T}} \hat{\boldsymbol{f}}, \tag{14}$$

where λ is a Lagrange multiplier. Note that this equation is equivalent to Phillips-Tikhonov regularization (with the discrepancy principle, i.e. $\left\| \hat{\boldsymbol{f}} - A\boldsymbol{f} \right\| \leq \|\varepsilon\|$, as constraint), and that the Lagrange multiplier plays the role of regularization parameter. The Lagrange multiplier is found by solving Eq. (14) iteratively until the constraint is matched.

Note that we only find one of the possible solutions to the problem, but that we know that the solution we find is the smoothest one, i.e. it is well possible that in reality there is more structure (more high spatial-frequency components), but not less (as long as our estimate of the measurement errors is realistic). In effect, thus, this method is similar to bandwidth limitation in Fourier techniques for deconvolution. The problem as described here is not well defined at the edges of the measurement region: not enough information is available to invert the problem there. The range of integral (11) was chosen to be the measurement region, which means that the region outside the measurement region has to be neglected (note that this is not the same as assuming that the measurements are zero there). Reasonable values are obtained, but the inverted values at the very edge should not be trusted. This situation can be improved if more is known about the values at the edges of the measurement region and this information is included in the object function $\langle \boldsymbol{f} | \Omega | \boldsymbol{f} \rangle$.

REFERENCES

1 A.G. Lindgren and P.A. Rattey, Advances in Electronics and Electron Physics **56**, 359 (1981)

2 A. Macovski, Proc. IEEE **71**, 373 (1983)

3 R.N. Bracewell, J. Comput. Assisted Tomogr. **1**, 6 (1977)

4 A. Holland and G.A. Navratil, Rev. Sci. Instrum. **57**, 1557 (1986)

5 A.R. Formiconi, A. Pupi and A. Passeri, Phys. Med. Biol. **34**, 69 (1989)

6 L.C. Ingesson *et al.*, in *Proc. 20th EPS Conf. on Controll. Fusion and Plasma Phys.*, Eds. J.A. Costa Cabral *et al.*, Europhysics Conference Abstracts Vol. 17C (EPS, 1993), Part III, pp. 1147

7 L.C. Ingesson *et al.*, *Projection-space methods to take into account beam-width effects in two-dimensional tomography algorithms*, Report JET-R(98)02 (JET Joint Undertaking, Abingdon, UK, 1998)

8 L.C. Ingesson *et al.*, in *Proc. 24th EPS Conf. on Controll. Fusion and Plasma Phys.*, Eds. M. Schittenhelm *et al.*, Europhysics Conference Abstracts Vol. 21A (EPS, 1997), Part I, pp. 113

[9] L.C. Ingesson *et al.*, in *Proc. 26th EPS Conf. On Controll. Fusion and Plasma Phys.*, Eds. B. Schweer *et al.*, Europhysics Conference Abstracts Vol. 23J (EPS, 1999), pp. 257

[10] L.C. Ingesson *et al.*, J. Opt. Soc. Am. A. **16**, 17 (1999)

[11] K.F. Mast *et al.*, Rev. Sci. Instrum. **62**, 744 (1991)

[12] R. Reichle *et al.*, in *Diagnostics for Experimental Thermonuclear Fusion Reactors*, Eds. P.E. Stott *et al.*, (Plenum Press, New York, 1996), pp. 559

[13] L.D. Horton *et al.*, Nucl. Fusion **39**, 1 (1999)

[14] J.J. Horan, *"The AΩ question,"* Appl. Opt. **14**, 2033 (1975)

[15] J.W. Beattie, IEEE Trans. Nucl. Sci. **NS-22**, 359 (1975)

[16] J.C. Verly, IEEE Trans. Med. Im. **MI-1**, 122–136 (1982)

[17] L.C. Ingesson and R. Reichle, *Lines of sight for ITER bolometers*, Report JET-R(98)03 (JET Joint Undertaking, Abingdon, UK, 1998)

[18] L.C. Ingesson, *Comparison of methods to determine the total radiated power in JET*, Report JET–R(99)06 (JET Joint Undertaking, Abingdon, UK, 1999)

[19] Y. Nagayama *et al.*, Jpn. J. Appl. Phys. **20**, L779 (1981)

[20] R. Reichle *et al.*, J. Nucl. Mat. **241–243**, 456 (1997)

[21] J.C. Fuchs *et al.*, in *Proc. 1998 Int. Conf. Plasma Phys.*, Ed. P. Pavlo, Europhysics Conference Abstracts Vol. 22C (EPS, 1998), pp. 1510

[22] M. Bertero, C. de Mol and E.R. Pikes, Inverse Problems **4**, 573 (1988)

[23] S. Twomey, *Introduction to the mathematics of inversion in remote sensing and indirect measurement* (Elsevier, Amsterdam and New York, 1977), pp. 124